

## Chapter 6

# GEOMETRIC MODELS FOR ANGLE AND TIME OF ARRIVAL

### 1. INTRODUCTION

Array antennas are sometimes employed at the receiver for a variety of purposes such as to combat fading or to reduce co-channel interference. To evaluate the performance of a wireless communication system using antenna arrays it becomes necessary to have spatial channel models that describe the angle of arrival and time of arrival of the multipath components. Among the most widely used radio propagation models is the single bounce scattering geometric model, where propagation between the transmitting and receiving antennas is assumed to take place via single scattering from an intervening obstacle. The scattering cross section of the scatterers is assumed to be isotropic, but their density is assumed to vary from location to location. Currently, several geometric models are available such as the ring model [53], discrete uniform model [118], circular scattering model [30], elliptical scattering model [98], Gaussian angle of arrival model [93], *etc.*, with each model being applicable to a specific environment type. For example, the circular scattering model is applicable to macro cell type of environments, whereas the elliptical model is suitable for a micro- or a pico-cell types of environment. Most of these models are 2D in nature in that they assume radio propagation to take place in a plane containing the transmitter and the receiver. In this Chapter we will consider the circular scattering model, the elliptical scattering model, and the Gaussian density model and show statistics for the angle and time of arrival.

## 2. GENERAL FORMULATION

Figure 6.1 shows the geometry of scatterers distributed around the mobile station which is transmitting to a base station. The scatter region is considered convex in shape and can possibly extend to infinity. It is assumed that propagation takes place in the horizontal plane containing the tip of the transmitting and receiving antennas. The global coordinates in this plane are denoted by  $(x, y)$ . The line joining the transmitter and receiver makes an angle  $\bar{\phi}$  with the  $x$ -axis and the coordinates of a point with respect to this line are  $(x_b, y_b)$ . The polar coordinates with respect to the base station are  $(r_b, \beta)$ . The mobile station is assumed to be located at a distance  $D$  from the base station along this line. The coordinates of a point with respect to the mobile station are denoted by  $(x_m, y_m)$ . The polar coordinates with respect to the mobile station are  $(r_m, \phi_m)$ . The relationships between these various coordinates are

$$x_b = r_b \cos \beta = x \cos \bar{\phi} + y \sin \bar{\phi}; \quad x_m = r_m \cos \phi_m = x_b - D \quad (6.1a)$$

$$y_b = r_b \sin \beta = -x \sin \bar{\phi} + y \cos \bar{\phi}; \quad y_m = r_m \sin \phi_m = y_b \quad (6.1b)$$

$$r_m^2 = r_b^2 + D^2 - 2r_b D \cos \beta; \quad \phi = \bar{\phi} + \beta. \quad (6.1c)$$

The density of scatterers about the mobile station is given as a probabil-

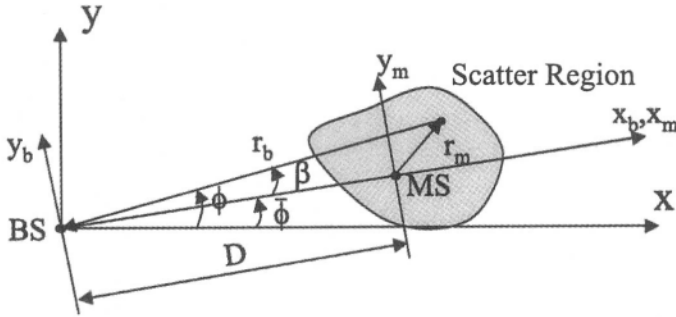


Figure 6.1. Geometrically based single bounce scattering model.

ity density function  $p_1(x_m, y_m)$ . Waves from the transmitter undergo single scattering from the scatter region before arriving at the receiver. The delay variable  $\tau$  is related to the total path length traveled  $r_b + r_m$  and the speed of light  $c$  via

$$c\tau = r_b + r_m \quad (6.2a)$$

$$= r_b + \sqrt{r_b^2 + D^2 - 2r_b D \cos \beta}. \quad (6.2b)$$

The locus of all points having a constant value of  $\tau$  is an ellipse with the base station and mobile station at its foci as shown in Figure 6.2. Waves arriving

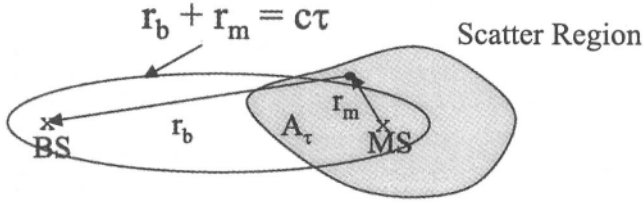


Figure 6.2. Waves arriving with delay less than  $\tau$  will arrive from the intersection of the ellipse and the scatter region.

from the scattering region that is enclosed by this ellipse will have delays less than  $\tau$ . Maximum delay  $\tau_M$  occurs when the ellipse just encloses all points of the scatter region. If the scattering region extends to infinity, the maximum delay becomes infinity.

The objective is to determine the marginal p.d.f.  $p(\beta)$  of the angle of arrival (AOA) and the marginal p.d.f.  $p(\tau)$  of the time of arrival (TOA) as seen from the base station given  $p_1(x_m, y_m)$ . It is assumed that the radiation patterns of the transmitting and receiving antennas are omnidirectional in the  $xy$  plane. This is not a serious limitation as the transmitting antenna pattern could always be included in the definition of  $p(x_m, y_m)$  and the receiving antenna pattern could always be included in  $p(\beta)$  and  $p(\tau)$ . The problem boils down to transformation of random variables from the Cartesian system  $(x_m, y_m)$  to the polar coordinate system  $(r_b, \beta)$  or to  $(\tau, \beta)$ . The joint density in  $(r_b, \beta)$  can be obtained from the standard Jacobian of the transformation between Cartesian and polar coordinates relating the elemental area  $dx_m dy_m = dx_b dy_b = r_b dr_b d\beta$ . The result is

$$p(r_b, \beta) = r_b p_1(x_m, y_m) \Big|_{\substack{x_m = r_b \cos \beta - D \\ y_m = r_b \sin \beta}} \tag{6.3}$$

A. PDF for AOA:

The marginal p.d.f.  $p(\beta)$  is obtained by including contribution from all points along the line  $\beta = \text{constant}$ . If this line intersects the scatter region at  $r_{bm}(\beta)$  and  $r_{bM}(\beta)$  with  $0 \leq r_{bm} \leq r_b \leq r_{bM} < \infty$ , then

$$p(\beta) = \int_{r_{bm}(\beta)}^{r_{bM}(\beta)} p(r_b, \beta) dr_b$$

$$= \int_{r_{bm}(\beta)}^{r_{bM}(\beta)} r_b p_1(r_b \cos \beta - D, r_b \sin \beta) dr_b. \quad (6.4)$$

It is of interest to determine the mean angle  $\bar{\beta}$  and the variance  $\tilde{\beta}^2$  for a given distribution. It is reasonable to assume that the scatter density is symmetrically distributed about the line joining the base station and the mobile. In this case the p.d.f.  $p(\beta)$  will be an even function in  $\beta$  and the mean angle  $\bar{\beta} = 0$ . The variance for a symmetric distribution is

$$\tilde{\beta}^2 = \int_{-\pi}^{\pi} \beta^2 p(\beta) d\beta. \quad (6.5)$$

Equation (6.5) can be cast in a different form by making use of Parseval's theorem for Fourier series. Expressing  $\beta^2$  and  $p(\beta)$  as a Fourier series in the interval  $(-\pi, \pi)$ , equation (6.5) can be expressed as

$$\tilde{\beta}^2 = \frac{\pi^2}{3} + 4\pi \sum_{n=1}^{\infty} (-1)^n \frac{B_n}{n^2}, \quad (6.6)$$

where the even p.d.f.  $p(\beta)$  is expressed as Fourier cosine series

$$p(\beta) = \frac{1}{2\pi} + \sum_{n=1}^{\infty} B_n \cos n\beta \quad (6.7)$$

with coefficients

$$B_n = \frac{2}{\pi} \int_0^{\pi} p(\beta) \cos n\beta d\beta. \quad (6.8)$$

Equation (6.6) is very convenient if the Fourier cosine coefficients of  $p(\beta)$  can be found in a closed form. The r.m.s. angular spread in a scattering environment is defined as  $2(\tilde{\beta} - \bar{\beta})$ .

In the study of array antennas, it is also of interest to determine the complex spatial correlation

$$\rho(\mathbf{k}_o d) = \langle e^{-j\mathbf{k}_o d \cos \phi} \rangle \quad (6.9)$$

between the field received at two points located along the  $x$ -axis and separated by a distance  $d$ . The quantity  $\mathbf{k}_o$  is the usual wavenumber in free-space and angle brackets denote expectation with respect to the angular variable  $\phi = \bar{\phi} + \beta$ . In Appendix B, it is shown that the expression for  $\rho(\mathbf{k}_o d)$  for

symmetric distributions, with  $p(-\beta) = p(\beta)$ , can also be put in the form:

$$\rho(k_o d) = \int_{-\pi}^{\pi} e^{-j k_o d \cos \bar{\phi} \cos \beta} \cos(k_o d \sin \bar{\phi} \sin \beta) p(\beta) d\beta \quad (6.10)$$

$$= J_0(k_o d) + 2\pi \sum_{n=1}^{\infty} (-j)^n J_n(k_o d) B_n \cos n\bar{\phi}, \quad (6.11)$$

where  $J_n(\cdot)$  is the Bessel function of the first kind of order  $n$ .

B. PDF for TOA:

The marginal p.d.f. for the time of arrival could, in principle, be obtained by first finding the joint density  $p(\tau, \beta)$  and integrating over all possible values of  $\beta(\tau)$ . However, a simpler approach is to first find the c.d.f.  $P(\tau)$  and then to take its derivative w.r.t.  $\tau$  to get  $p(\tau)$  [30]. To determine the c.d.f. for a particular  $\tau$  it is essential to consider all delays that are less than  $\tau$ . All points of the scatter region that lie within the ellipse  $r_b + r_m = c\tau$  will contribute to this. Denoting the intersection of the scatter region with the ellipse as  $A_\tau$ , the c.d.f. and the p.d.f. for the time of arrival are

$$P(\tau) = \iint_{A_\tau} p_1(x_m, y_m) dx_m dy_m \quad (6.12)$$

$$p(\tau) = \frac{d}{d\tau} \iint_{A_\tau} p_1(x_m, y_m) dx_m dy_m \quad (6.13)$$

The mean delay  $\bar{\tau}$  and the second moment of the delay  $\overline{\tau^2}$  can be determined from

$$\bar{\tau} = \int \tau p(\tau) d\tau \quad (6.14)$$

$$\overline{\tau^2} = \int \tau^2 p(\tau) d\tau \quad (6.15)$$

### 3. ELLIPTICAL SCATTERING MODEL

In this model, first described in [78], the scatter density is assumed to be uniform inside an elliptical region of maximum delay  $\tau_M$ , with foci at the base station and the mobile. The semi-major axis  $a$  of the ellipse is  $c\tau_M/2$  and the semi-minor axis  $b$  is equal to  $\sqrt{a^2 - (D/2)^2}$ . The area of the ellipse is  $A_e = \pi ab$ . The equation of the ellipse in polar coordinates is

$$r_{be} = \frac{4a^2 - D^2}{4a - 2D \cos \beta}. \quad (6.16)$$

Figure 6.3 shows the geometry of the elliptical scattering model.

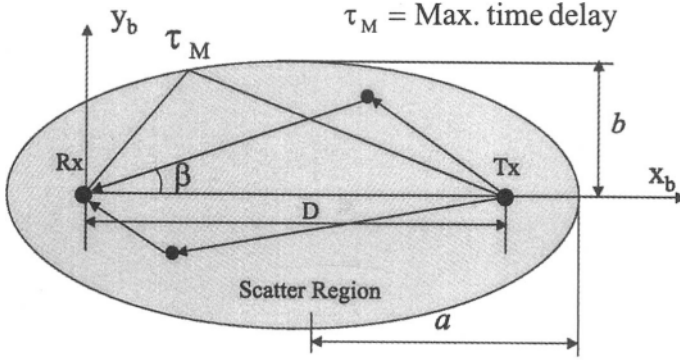


Figure 6.3. Elliptical Scattering Model having two parameters  $D$  and  $\tau_M$ .

The model is appropriate for microcell environments where the antenna heights are relative low. With low antennas, the base station will receive multipath components from scatterers distributed around the mobile as well as itself. All angles in the azimuth plane are involved so that  $-\pi \leq \beta \leq \pi$ . Furthermore, the maximum delay is set by the size of the ellipse. On physical grounds, the assumption of the model that delays greater than  $\tau_M$  are non-existent may be justified by the fact that longer delays will have weaker strength owing to the longer path length traveled.

The scatter density  $p_1(x_m, y_m)$  within this elliptical region is equal to

$$p_1(x_m, y_m) = \frac{1}{A_e}. \quad (6.17)$$

For the elliptical scatter region the lower and upper limits in (6.4) are  $r_{bm} = 0$ ,  $r_{bM} = r_{be}$ . Substituting these and (6.17) into (6.4) and carrying out the integration and simplifying, the p.d.f. for the angle of arrival for the elliptical scattering model  $p_e(\beta)$  is

$$p_e(\beta) = \frac{r_{be}^2}{2A_e} = \frac{a}{b} \frac{1}{2\pi} \left[ \frac{1 - (D/2a)^2}{1 - (D/2a) \cos \beta} \right]^2, \quad -\pi \leq \beta \leq \pi \quad (6.18)$$

$$\triangleq \frac{k_1}{[1 - (D/2a) \cos \beta]^2} \quad (6.19)$$

where

$$k_1 = \frac{a}{2\pi b} \left[ 1 - \left( \frac{D}{2a} \right)^2 \right]^2. \tag{6.20}$$

For this p.d.f., the mean angle  $\bar{\beta}$  is clearly zero. The Fourier cosine coefficients can be determined by the application of the identity [43, 3.616-7]

$$\int_0^\pi \frac{\cos nx}{(1 - 2\alpha \cos x + \alpha^2)^2} dx = \frac{\pi}{\alpha^n(\alpha^2 - 1)^2} \left[ n + \frac{\alpha^2 + 1}{\alpha^2 - 1} \right]. \tag{6.21}$$

Applying the above identity to (6.8) and simplifying, the Fourier cosine coefficients are

$$B_n = \frac{a \cos^2 \beta_1}{\pi^2 b} \left( \frac{\sin \beta_1}{1 + \cos \beta_1} \right)^n \left( n + \frac{1}{\cos \beta_1} \right) \tag{6.22}$$

where

$$\sin \beta_1 \triangleq \frac{D}{2a} < 1 \implies b = a \cos \beta_1. \tag{6.23}$$

Substituting (6.22) into (6.6), the standard deviation  $\tilde{\beta}$  for the elliptical scatter model is

$$\begin{aligned} \tilde{\beta} &= \left[ \frac{\pi^2}{3} + \frac{4a}{b} \cos^2 \beta_1 \sum_{n=1}^\infty \frac{1}{n^2} \times \right. \\ &\quad \left. \times \left( \frac{-\sin \beta_1}{1 + \cos \beta_1} \right)^n \left( n + \frac{1}{\cos \beta_1} \right) \right]^{1/2} \\ &= \left[ \frac{\pi^2}{3} + 4 \cos \beta_1 \ln \left( \frac{1 + \cos \beta_1}{1 + \cos \beta_1 + \sin \beta_1} \right) + \right. \\ &\quad \left. + 4 \sum_{n=1}^\infty \left( \frac{-\sin \beta_1}{1 + \cos \beta_1} \right)^n \frac{1}{n^2} \right]^{1/2}, \tag{6.24} \end{aligned}$$

where the identity [43, 1.513-4]

$$\ln(1 - x) = - \sum_{n=1}^\infty \frac{x^n}{n}$$

was used in (6.24). The r.m.s. angular spread is  $2\tilde{\beta}$ . The Fourier coefficients can be substituted in (6.11) to yield the spatial cross correlation.

The c.d.f. for the time of arrival for a given  $\tau$  is obtained by inserting (6.17) into (6.12). The ellipse with delay  $\tau$  will have a semi-major axis  $a_\tau = c\tau/2$  and a semi-minor axis  $b_\tau = \sqrt{a_\tau^2 - (D/2)^2}$ . Intersection of the

ellipse with delay  $\tau$  with the scatter region is simply the ellipse itself. Because of the uniform density, the integral in (6.12) is simply equal to the area of ellipse  $A_\tau = \pi a_\tau b_\tau$ . The c.d.f. in the time of arrival is

$$P_e(\tau) = \frac{A_\tau}{A_e} = \frac{a_\tau b_\tau}{ab} = \frac{\tau}{\tau_M} \sqrt{\frac{(\tau/\tau_M)^2 - (D/2a)^2}{1 - (D/2a)^2}}. \quad (6.25)$$

Differentiating  $P_e(\tau)$  w.r.t. yields the p.d.f.  $p_e(\tau)$  as

$$p_e(\tau) = \frac{1}{\tau_M} \frac{a}{b} \frac{2(\tau/\tau_M)^2 - (D/2a)^2}{\sqrt{(\tau/\tau_M)^2 - (D/2a)^2}}, \quad \frac{D}{2a} \leq \frac{\tau}{\tau_M} \leq 1. \quad (6.26)$$

The p.d.f. is peaked and has an integrable singularity at  $\tau/\tau_M = D/2a$  or at  $\tau = D/c$ . This peak corresponds to the line of sight path. The mean delay  $\bar{\tau}$  for the model can be found from (6.14)

$$\begin{aligned} \bar{\tau} &= \frac{a}{b} \tau_M \int_{D/2a}^1 x \frac{2x^2 - (D/2a)^2}{\sqrt{x^2 - (D/2a)^2}} dx \\ &= \frac{a}{3b} \tau_M \sqrt{1 - \left(\frac{D}{2a}\right)^2} \left[ 2 + \left(\frac{D}{2a}\right)^2 \right] \\ &= \tau_M \left( 1 - \frac{\cos^2 \beta_1}{3} \right). \end{aligned} \quad (6.27)$$

Likewise, the second moment  $\overline{\tau^2}$  can be found from (6.15)

$$\begin{aligned} \overline{\tau^2} &= \frac{a}{b} \tau_M^2 \int_{D/2a}^1 x^2 \frac{2x^2 - (D/2a)^2}{\sqrt{x^2 - (D/2a)^2}} dx \\ &= \frac{a}{b} \tau_M^2 \left[ 2 \int_0^{\cos \beta_1} (y^2 + \sin^2 \beta_1)^{3/2} dy \right. \\ &\quad \left. - \sin^2 \beta_1 \int_0^{\cos \beta_1} (y^2 + \sin^2 \beta_1)^{1/2} dy \right] \\ &= \frac{\tau_M^2}{4} \left[ 2 + \sin^2 \beta_1 + \sin^3 \beta_1 \tan \beta_1 \ln \left( \frac{1 + \cos \beta_1}{\sin \beta_1} \right) \right]. \end{aligned} \quad (6.28)$$

The r.m.s. delay spread for the elliptical scattering model can be found from  $\bar{\tau} = \sqrt{\overline{\tau^2} - \bar{\tau}^2}$ . Figure 6.4 shows the p.d.f. of the angle of arrival and

Figure 6.5 shows a plot of  $\tau_M p_e(\tau)$  for the elliptical scattering model for  $D = 1000$  m and  $\tau_M = 5 \mu\text{s}$ . For these parameters, the r.m.s. angular spread from (6.24) is  $2 \times 55^\circ = 110^\circ$ . The mean delay from 6.27) is  $4.0741 \mu\text{s}$  and the second moment in the delay variable from (6.28) is  $0.675\tau_M^2$ . The r.m.s. delay spread is  $0.523 \mu\text{s}$ .

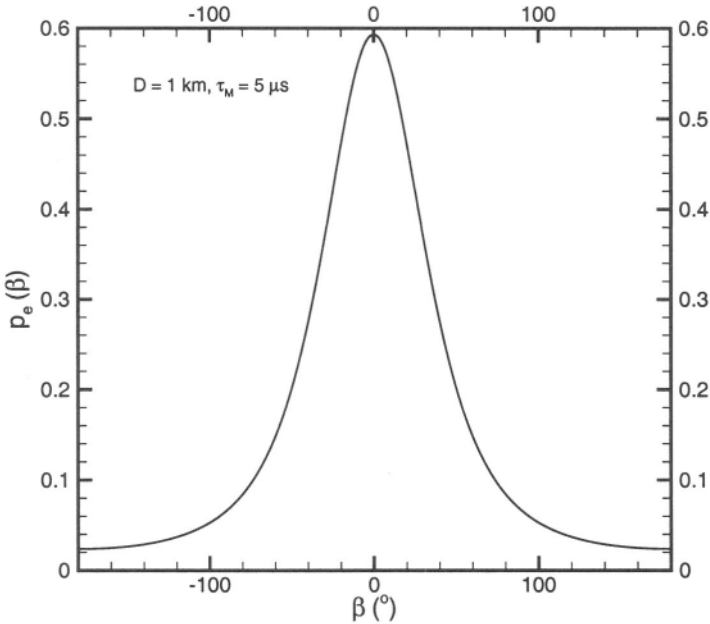


Figure 6.4. PDF of the angle of arrival for the elliptical scattering model. Standard deviation in angle is  $\tilde{\beta} = 55^\circ$ .

Figure 6.6 shows the variation of the r.m.s. angular spread and r.m.s. delay spread with increasing size of scatter region. The size of the elliptical scatter region is increased by increasing  $\tau_M$  and maintaining the distance between the transmitter and receiver fixed at 1 km. It is seen that while both the angular spread and the delay spread increase with the ellipse size, the delay spread increases more or less linearly with increasing  $\tau_M$ .

#### 4. CIRCULAR SCATTERING MODEL

The next model we consider is the circular scattering model where the scatter density is uniformly distributed inside a circular region of radius  $R$

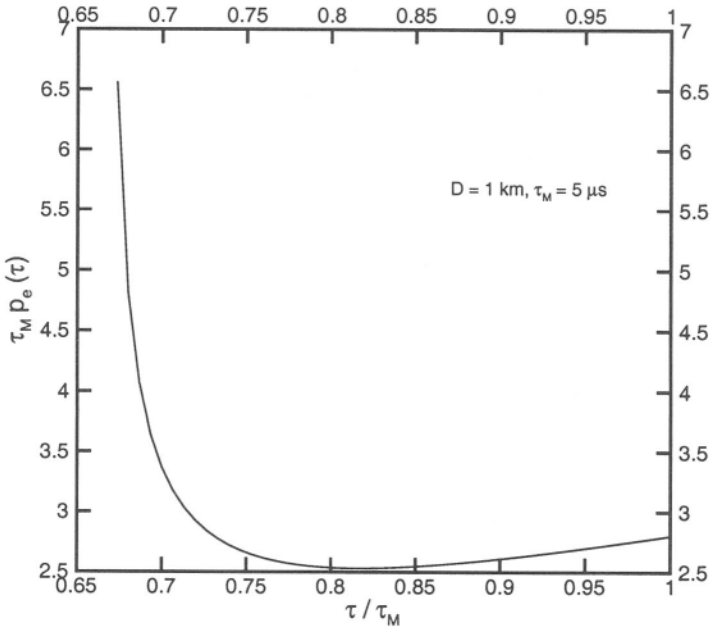


Figure 6.5. Plot of  $\tau_M p_e(\tau)$  versus  $\tau/\tau_M$  for the elliptical scattering model. The mean delay is  $0.815\tau_M$  and the second moment is  $0.675\tau_M^2$ . RMS delay spread is  $0.523\mu\text{ s}$ .

about the mobile. Such a model is appropriate for macrocell environments where the base station antenna height is relatively high that no significant scatterers lie around it. It is assumed in the following that  $R < D$  although the converse situation can also be handled similarly. Figure 6.7 shows the geometry of the circular scattering model. The area of the scatter region is  $A_c = \pi R^2$ . The p.d.f. of the scatter density is

$$p_1(x_m, y_m) = \frac{1}{A_c}. \quad (6.29)$$

Substituting  $r_m = R$ , the points of intersection of the line  $\beta = \text{constant}$  with the circle are found to be

$$r_{bm} = D \cos \beta - \sqrt{D^2 \cos^2 \beta - D^2 + R^2} \quad (6.30)$$

$$r_{bM} = D \cos \beta + \sqrt{D^2 \cos^2 \beta - D^2 + R^2} \quad (6.31)$$

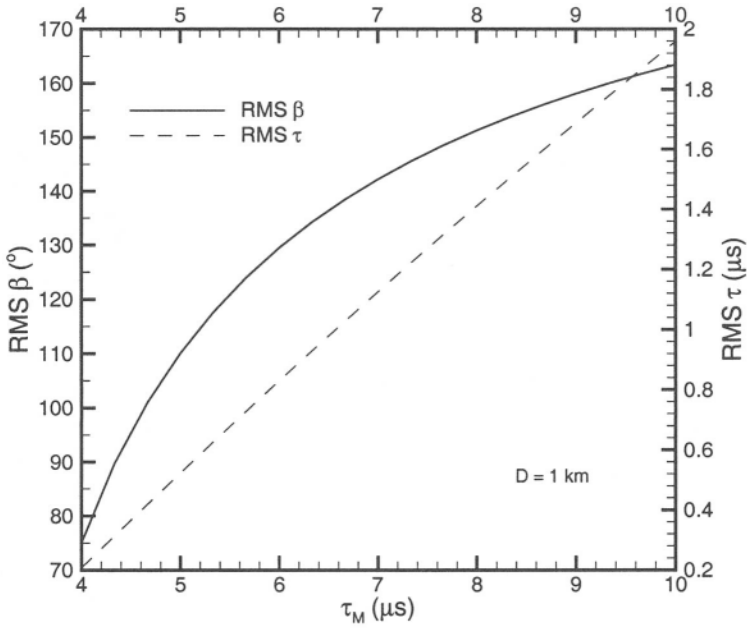


Figure 6.6. Plot of r.m.s. angular spread and r.m.s. delay spread as a function of maximum delay  $\tau_M$  for the elliptical scattering model.

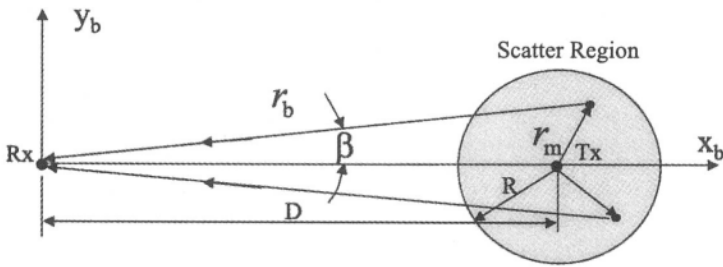


Figure 6.7. Circular Scattering Model having two parameters  $D$  and  $R$ .

Substituting these and (6.29) into (6.4), we get the p.d.f.  $p_c(\beta)$  for the angle of arrival:

$$p_c(\beta) = \frac{r_{bM}^2 - r_{bm}^2}{2A_c}$$

$$= \frac{2 \cos \beta \sqrt{\sin^2 \xi - \sin^2 \beta}}{\pi \sin^2 \xi}, \quad -\xi \leq \beta \leq \xi, \quad (6.32)$$

where  $\sin \xi = R/D$ . The mean angle is once again zero. Because the Fourier coefficients of (6.32) are difficult to find, we will proceed directly with the definition (6.5) to determine the variance of the angular spread.

$$\tilde{\beta}^2 = \frac{2}{\pi \sin^2 \xi} \int_{-\xi}^{\xi} \beta^2 \cos \beta \sqrt{\sin^2 \xi - \sin^2 \beta} d\beta. \quad (6.33)$$

Making a change of variable  $\sin \beta = \sin \xi \sin \theta$  yields

$$\tilde{\beta}^2 = \frac{4}{\pi} \int_0^{\pi/2} \left[ \sin^{-1}(\sin \xi \sin \theta) \right]^2 \cos^2 \theta d\theta. \quad (6.34)$$

Using the series representation [43, 1.645-2] for  $(\sin^{-1}(x))^2$  and using the formulas [43, 3.621-5, 8.384-1, 8.339-2] and the definition

$$(2k)!! = 2 \cdot 4 \cdot 6 \cdot \dots \cdot 2k = 2^k k!, \quad (6.35)$$

the result for the variance is

$$\tilde{\beta}^2 = \frac{\sin^2 \xi}{2} \sum_{k=0}^{\infty} \frac{\sin^{2k} \xi}{(k+1)^2 (k+2)} \quad (6.36)$$

$$\approx \left( \frac{\sin \xi}{2} \right)^2, \quad \sin \xi \leq 0.8, \quad (6.37)$$

where the approximate formula is just the first term of the infinite series. The r.m.s. angular spread is  $2\tilde{\beta}$ . Figure 6.9 shows the r.m.s. angular spread computed by the exact (6.36) and the approximate (6.37) formulas. The sum for the exact calculation included 11 terms. Also shown in the plot is the % error incurred by using the approximate formula. It is seen that even for  $R/D = 1$  the error is less than 12%. For  $R/D < 0.8$ , the error in the approximate formula is  $< 6\%$ .

A closed form expression for the complex correlation function for general  $\bar{\phi}$  is difficult to obtain. It can always be computed by inserting the p.d.f. (6.32) into (6.10) and numerically evaluating the integral. However, for  $\bar{\phi} = \pi/2$ , *i.e.*, when the line joining the transmitter and receiver is perpendicular to the axis along which spatial correlation is being evaluated, the integral can be

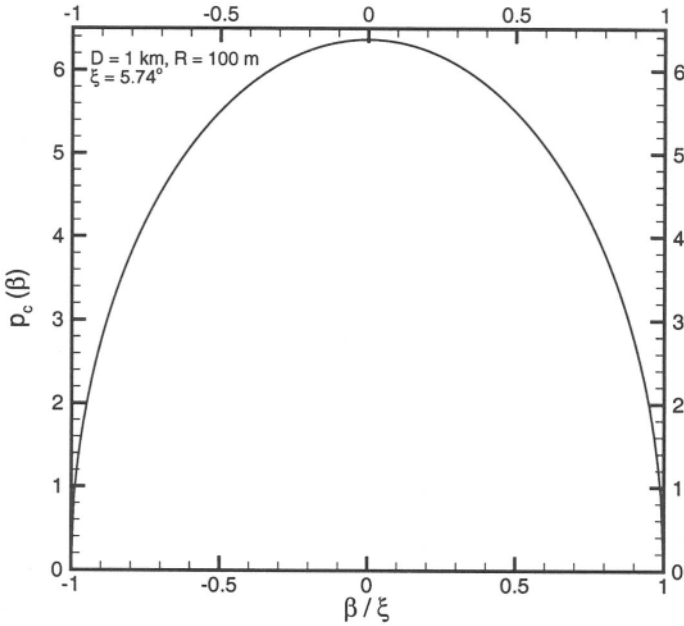


Figure 6.8. Plot of  $p_c(\beta)$  versus  $\beta/\xi$  for the circular scattering model with  $D = 1$  km,  $R = 100$  m  $\implies \xi \approx 5.74^\circ$ .

performed in a closed form. For  $\bar{\phi} = \pi/2$ , equation (6.10) yields

$$\begin{aligned}
 \rho(k_0 d) &= \int_{-\xi}^{\xi} p_c(\beta) \cos(k_0 d \sin \beta) d\beta \\
 &= \frac{4}{\pi} \int_0^1 \sqrt{1-t^2} \cos(tk_0 d \sin \xi) dt, \quad \text{where } \sin \beta = t \sin \xi \\
 &= \frac{2J_1(k_0 d \sin \xi)}{k_0 d \sin \xi} \quad (\text{from [43, 3.771-8]}). \tag{6.38}
 \end{aligned}$$

Like the elliptical scattering model, constant value of the scatter density within the region enables the determination of the c.d.f. for the time of arrival by simply finding the area of the scatter region enclosed by the ellipse  $r_b + r_m = c\tau$  and dividing that area by  $A_c$ . The enclosed area is shown with hatch lines in Figure 6.10. The c.d.f.  $P_c(\tau)$  is [30]

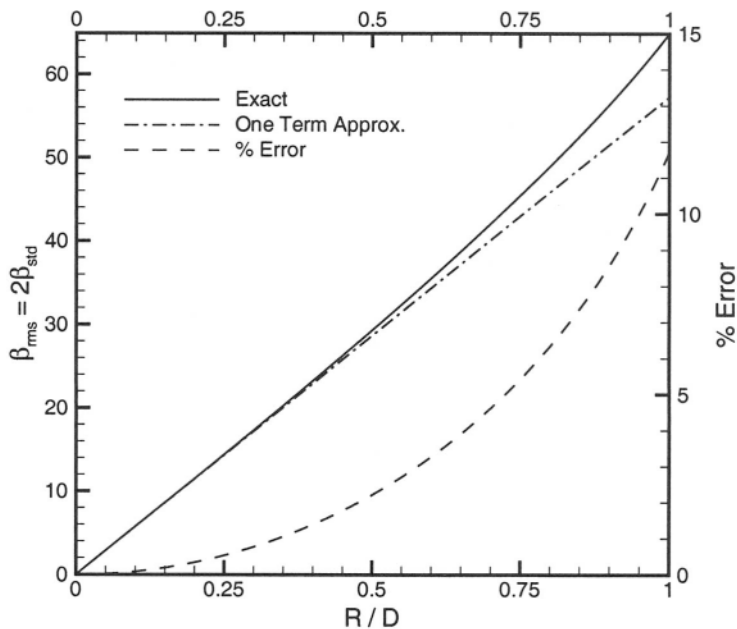


Figure 6.9. Plot of the r.m.s. angular spread  $2\tilde{\beta}$  versus  $R/D$  for the circular scattering model. Also shown is the % error incurred in using the approximate formula.

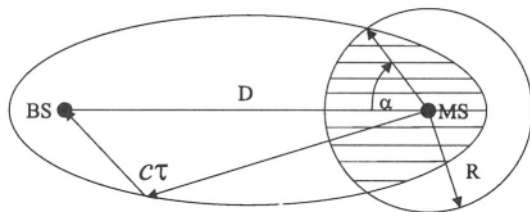


Figure 6.10. Calculation of the area for finding c.d.f. of TOA in the circular scattering model.

$$P_c(\tau) = \frac{\alpha}{\pi} + \frac{1}{\pi R^2} \int_{\alpha}^{\pi} \left( \frac{c^2 \tau^2 - D^2}{2c\tau - 2D \cos \theta} \right)^2 d\theta, \quad (6.39)$$

where the angle  $\alpha$ , shown in Figure 6.10, is defined as

$$\cos \alpha = \frac{D^2 + 2Rc\tau - (c\tau)^2}{2RD}. \quad (6.40)$$

The first part on the right hand side of (6.39) corresponds to the fractional area of the circular sector contained within  $\pm\alpha$ , and the integral corresponds to the remaining area. When the angle  $\alpha$  becomes equal to  $\pi$ , all of the circular region will be enclosed by the ellipse and  $P_c(\tau) = 1$ . This will happen for  $c\tau = D + 2R \triangleq c\tau_M$ . The p.d.f.  $p_c(\tau)$  of the time of arrival is found by differentiating (6.39) w.r.t.  $\tau$ . Denoting

$$D = c\tau_o \tag{6.41}$$

$$\tau = \tau_o \cosh \gamma, 0 \leq \gamma \leq \gamma_M \implies \frac{d\gamma}{d\tau} = \frac{1}{\tau_o \sinh \gamma} \tag{6.42}$$

where

$$\tau_M = \tau_o \cosh \gamma_M \implies \cosh \gamma_M = 1 + 2 \sin \xi, \tag{6.43}$$

the p.d.f. of the time of arrival for the circular scattering model is

$$p_c(\tau) = \frac{1}{2\pi\tau_o \sin^2 \xi \sinh \gamma} \left[ \frac{\sin \xi \sin \alpha (\cosh \gamma_M - \cosh \gamma - 1)}{\sinh \gamma} + (2 \cosh^2 \gamma - 1) \tan^{-1} \left( \frac{\sinh \gamma (\cosh \gamma_M - \cosh \gamma)}{2 \sin \xi \sinh \gamma} \right) \right] \tag{6.44}$$

The p.d.f. will have an integrable singularity at  $\gamma = 0$  or for  $\tau = \tau_o$  corresponding to the line of sight path. For  $\tau > \tau_M$ , the p.d.f. will be equal to zero. Figure 6.11 shows a plot of the p.d.f.  $p_c(\tau)$  as a function of  $\tau/\tau_o$  for  $D = 1$  km and  $R = 100$  m. Note that the p.d.f. is peaked at  $\tau = \tau_o$ . The mean and the second moment of the delay can be numerically computed from the definitions (6.14) and (6.15). For the parameters chosen above, the mean delay  $\bar{\tau}$  is  $3.5163 \mu\text{s}$  and the r.m.s. delay spread is  $0.443 \mu\text{s}$ .

## 5. GAUSSIAN SCATTER DENSITY

In this model the scatter density around the mobile is assumed to follow a Gaussian distribution. The model was first considered by Fuhl [38], but exact analytical results were not available until recently [60]. The scatter density is given as

$$p_1(x_m, y_m) = \frac{1}{2\pi\sigma_s^2} e^{-r_m^2/2\sigma_s^2}, \tag{6.45}$$

where the standard deviation  $\sigma_s$  is a measure of the width of the scatter region. Figure 6.12 shows the geometry of the scattering region. The effective width of the scattering region could potentially extend to infinity. For a given

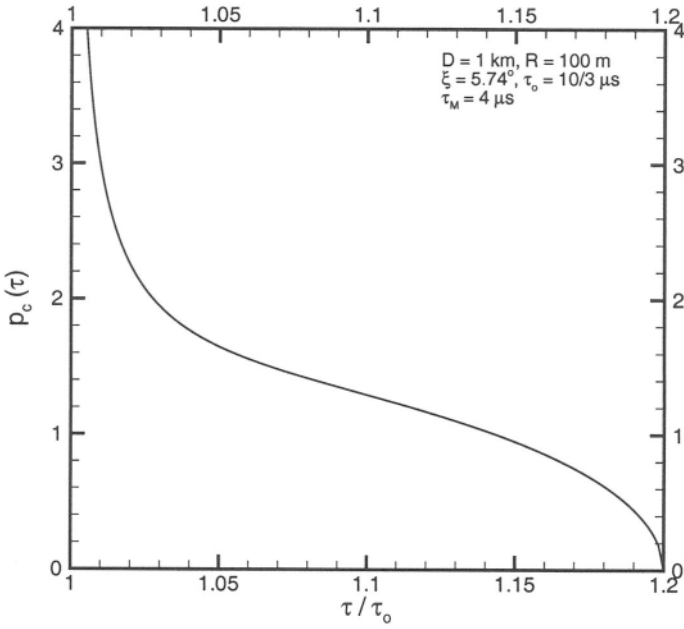


Figure 6.11. Plot of the p.d.f. of the time of arrival for the circular scattering model.

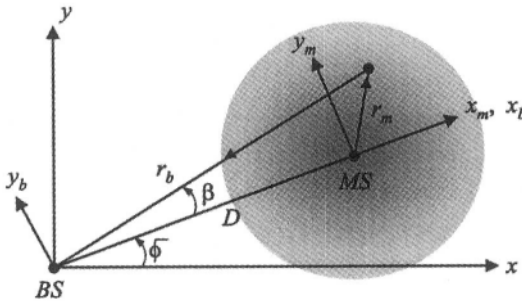


Figure 6.12. Gaussian density profile around a mobile station.

distance  $D$  between the transmitter and receiver, a small  $\sigma_s$  would primarily include only scatterers near the mobile. By making  $\sigma_s$  larger, more and more scatterers near the base station could also be included. Hence the model is appropriate both for microcells and macrocells. The p.d.f.  $p_g(\beta)$  for the angle of arrival could be obtained by substituting (6.45) into (6.4) and noting that

$r_m^2 = (r_b - D \cos \beta)^2 + D^2 \sin^2 \beta$ ,  $r_{bm} = 0$  and  $r_{bM} \rightarrow \infty$ , Figure 6.13:

$$p_g(\beta) = \frac{e^{-\frac{D^2 \sin^2 \beta}{2\sigma_s^2}}}{2\pi\sigma_s^2} \int_0^\infty r_b e^{-(r_b - D \cos \beta)^2 / 2\sigma_s^2} dr_b. \quad (6.46)$$

The integral could be carried out in a closed form through some elementary manipulations with the result

$$p_g(\beta) = \frac{1}{2\pi} e^{-\frac{D^2}{2\sigma_s^2}} + \frac{D \cos \beta}{\sigma_s 2\sqrt{2\pi}} e^{-\frac{D^2 \sin^2 \beta}{2\sigma_s^2}} \operatorname{erfc}\left(-\frac{D \cos \beta}{\sqrt{2}\sigma_s}\right), \quad (6.47)$$

where  $\operatorname{erfc}(\cdot)$  is the usual complementary error function defined in (4.109) of Chapter 4. The p.d.f. is seen to depend on the single parameter  $D/\sigma_s$ . For

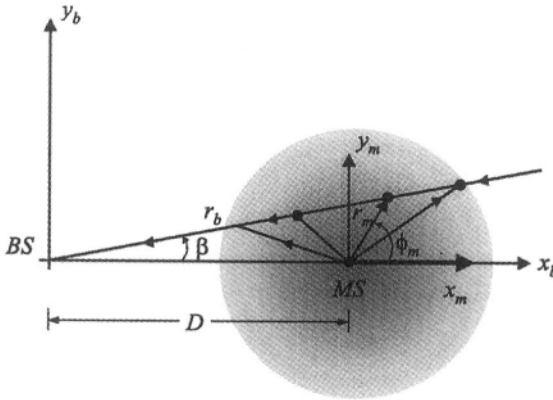


Figure 6.13. Geometry used in the calculation of the p.d.f. of the angle of arrival for the Gaussian density model.

large  $D/\sigma_s$ , the factor involving the complementary error functions approaches a non-zero constant for  $\beta$  near zero and approaches zero for  $\beta$  near  $\pi$ . Hence the p.d.f. behaves like a Gaussian function in  $\beta$  for small  $|\beta|$  and a constant value for  $|\beta| \sim \pi$ . Figure 6.14 shows the p.d.f. in the angle of arrival for  $D/\sigma_s = 1$  and 2. To determine the Fourier cosine coefficients  $B_n$  of  $p_g(\beta)$ , the integral form (6.46) is used in (6.8):

$$B_n = \frac{1}{2\pi\sigma_s^2} \frac{2}{\pi} \int_0^\pi \cos n\beta d\beta \int_0^\infty r_b e^{-(r_b^2 + D^2 - 2r_b D \cos \beta) / 2\sigma_s^2} dr_b. \quad (6.48)$$

Interchanging the order of integration and evaluating the integral w.r.t.  $\beta$  by

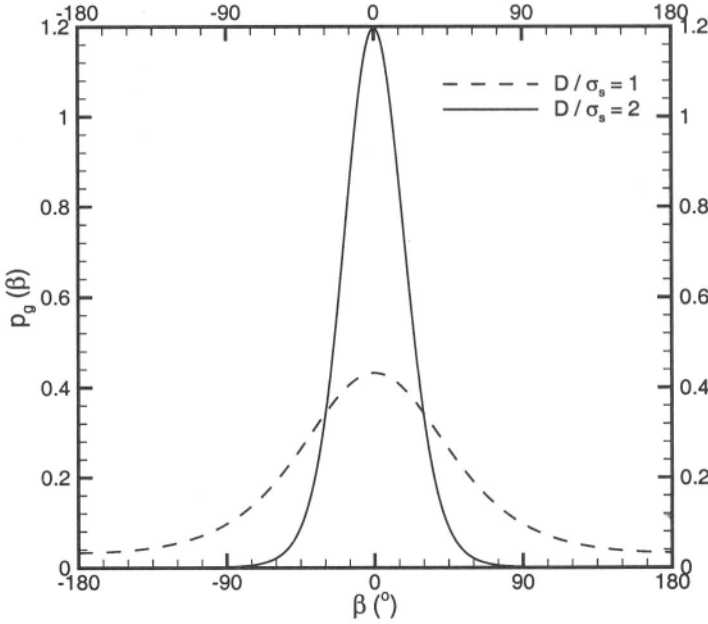


Figure 6.14. Plot of the p.d.f. of the angle of arrival for the Gaussian scattering model.

the formula [43, 8.431-5] results in

$$B_n = \frac{1}{\pi\sigma_s^2} \int_0^\infty r_b e^{-(r_b^2 + D^2)/2\sigma_s^2} I_n\left(\frac{r_b D}{\sigma_s^2}\right) dr_b, \quad (6.49)$$

where  $I_n(\cdot)$  is the modified Bessel function of the first kind of order  $n$ . The integral w.r.t.  $r_b$  can be carried out by first integrating by parts and then applying the identity [43, 6.618-4] to finally result in

$$B_n = \frac{D}{\sigma_s 2\sqrt{2\pi}} e^{-\frac{D^2}{4\sigma_s^2}} \left[ I_{\frac{n+1}{2}}\left(\frac{D^2}{4\sigma_s^2}\right) + I_{\frac{n-1}{2}}\left(\frac{D^2}{4\sigma_s^2}\right) \right]. \quad (6.50)$$

These coefficients may then be used in (6.6) and (6.11) to determine the r.m.s. angular spread and spatial correlation for the Gaussian scattering model. The respective series converge due to the following asymptotic behavior of the modified Bessel functions

$$I_n(x) \sim \frac{1}{\sqrt{2\pi n}} \left(\frac{xe}{2n}\right)^n, \quad n \rightarrow \infty. \quad (6.51)$$

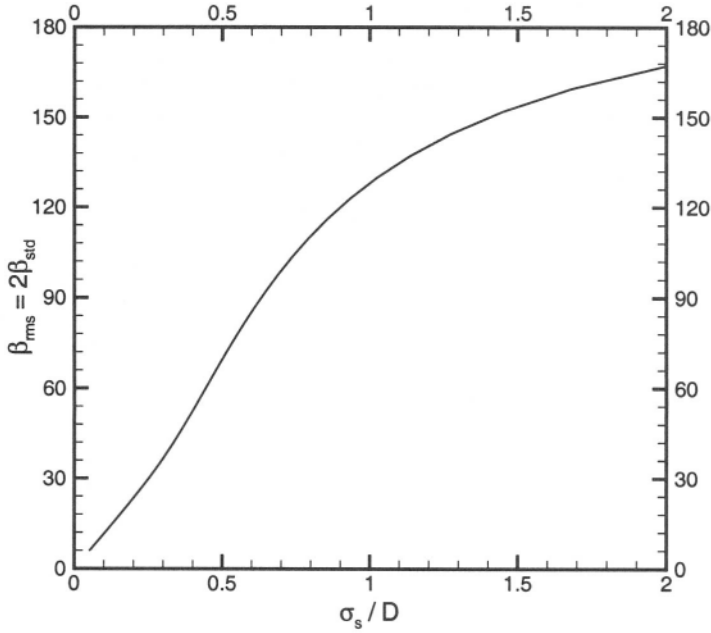


Figure 6.15. RMS angular spread for the Gaussian scattering model as a function of  $\sigma_s/D$ .

Figure 6.15 shows the r.m.s. angular spread  $2\tilde{\beta}$  as a function of  $\sigma_s/D$ . Over the range  $0 \leq \sigma_s/D \leq 2$ , the r.m.s. angular spread varies from  $0^\circ$  to about  $170^\circ$ . Expression for the spatial correlation is given in Appendix B.

As in the previous two cases, the p.d.f. in the time of arrival is determined from (6.13). Because the density extends over all space, the entire interior region of the ellipse  $r_b + r_m = c\tau$  is involved in the integrals, Figure 6.16. However, as  $p_1(x_m, y_m)$  is not a constant as in the previous two cases, evaluation of the integrals is no longer easy. The two dimensional integral can be converted into a one dimensional integral by evaluating it by integration by parts after a change of variable. Denoting  $D/\sigma_s = D_s$ ,  $D/c = \tau_o$  and  $\tau/\tau_o = \tau_n$ , the final result is [60]

$$\begin{aligned}
 p_g(\tau) = & \frac{1}{2\pi\tau_o} D_s^2 \frac{\exp(-D_s^2 \tau_n^2 / 8)}{\sqrt{\tau_n^2 - 1}} \times \\
 & \times \int_0^{\pi/2} [\tau_n^2 - \sin^2 \theta] e^{-\frac{D_s^2 \sin^2 \theta}{8}} \cosh\left(\frac{\tau_n D_s^2 \sin^2 \theta}{4}\right) d\theta. \quad (6.52)
 \end{aligned}$$



[43]. Applying these and denoting

$$\int_0^{\pi/2} g(\theta) d\theta = \frac{D_s^2}{4\tau_o} \frac{e^{-\frac{D_s^2 \tau_n^2}{8}}}{\sqrt{\tau_n^2 - 1}} \times \left[ \frac{I_1(D_s^2 \tau_n/4)}{D_s^2 \tau_n/4} + (\tau_n^2 - 1) I_0(D_s^2 \tau_n/4) \right] \triangleq p_{go}(\tau), \tag{6.54}$$

the following inequalities apply to  $p_g(\tau)$ :

$$p_{go}(\tau) e^{-D_s^2/8} \leq p_g(\tau) \leq p_{go}(\tau). \tag{6.55}$$

Figure 6.17 also shows the upper and lower bounds for  $D_s = 1$  and 2. The bounds are tight for small values of  $D_s$ . For large values of  $D_s$ , the lower bound is tighter than the upper one, although it is not apparent for  $D_s = 2$ .

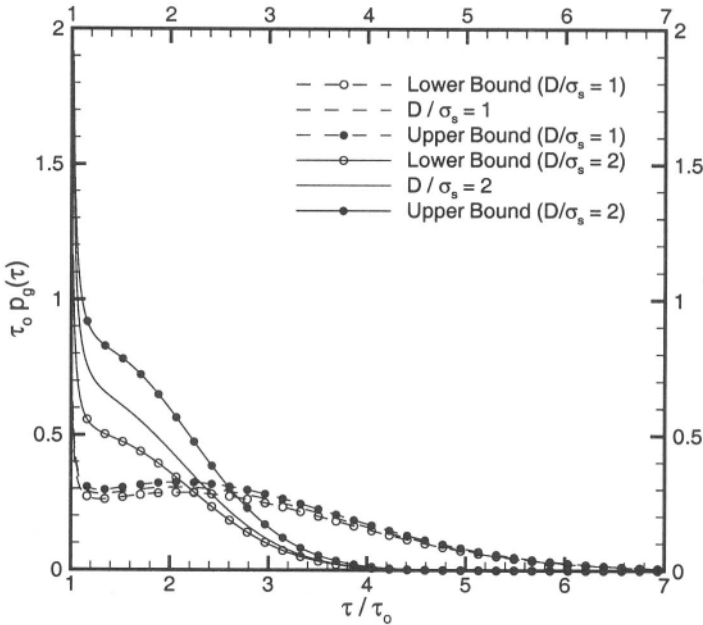


Figure 6.17. Plot of  $\tau_o p_g(\tau)$  for the Gaussian scattering model.

## 6. SUMMARY

This chapter dealt with a statistical description of several geometric scattering models: the elliptical scattering model, the circular scattering model, and the Gaussian density model. These models are very useful in simulation studies of wireless communication systems in a variety of scenarios. The quantities of interest in these models are the probability density functions for the angle of arrival and time of arrival. The elliptical scattering model is appropriate for microcells where both the transmitting and receiving antennas are embedded in a scattering environment. The circular scattering model is more suitable for a macrocell type of environment where one antenna (the base-station antenna) is placed well above the surrounding clutter. In such a case only scatterers in the vicinity of the low-lying mobile antenna are important. By varying the standard deviation of the Gaussian density function, the extent of significant scatterers around the mobile can be varied in a Gaussian density model, and the model finds use both in a microcell as well as in a macrocell environment.